

Article

The Structure and Optical Properties of Luminescent Europium Terephthalate Antenna Metal–Organic Frameworks Doped by Yttrium, Gadolinium, and Lanthanum Ions

Oleg S. Butorlin ¹, Anna S. Petrova ¹, Yulia N. Toikka ¹, Ilya E. Kolesnikov ¹, Sergey N. Orlov ^{1,2}, Mikhail N. Ryazantsev ^{1,3}, Nikita A. Bogachev ¹, Mikhail Yu. Skripkin ¹ and Andrey S. Mereshchenko ^{1,*}

- ¹ Saint Petersburg State University, 7/9 Universitetskaya emb., Saint Petersburg 199034, Russia; olbuse@mail.ru (O.S.B.); an.petra04.floreo@gmail.com (A.S.P.); helmi24@mail.ru (Y.N.T.); ilya.kolesnikov@spbu.ru (I.E.K.); orlov.s.n.1989@yandex.ru (S.N.O.); mikhail.n.ryazantsev@gmail.com (M.N.R.); n.bogachev@spbu.ru (N.A.B.); skripkin1965@yandex.ru (M.Y.S.)
- ² Institute of Nuclear Industry, Peter the Great St. Petersburg Polytechnic University (SPbSU), 29, Polytechnicheskaya Street, Saint Petersburg 195251, Russia
- ³ Nanotechnology Research and Education Centre RAS, Saint Petersburg Academic University, ul. Khlopina 8/3, Saint Petersburg 194021, Russia
- * Correspondence: a.mereshchenko@spbu.ru; Tel.: +7-951-677-5465

Abstract: New heterometallic antenna terephthalate MOFs, namely, $(Eu_xM_{1-x})_2bdc_3 \cdot 4H_2O$ ($M = Y, La, Gd$) ($x = 0.001-1$), were synthesized by a one-step method from aqueous solutions. The resulting compounds are isomorphic to each other; the crystalline phase corresponds to $Ln_2bdc_3 \cdot 4H_2O$. Upon 300 nm excitation to the singlet excited state of terephthalate ions, all compounds exhibit a bright red emission corresponding to the of ${}^5D_0-{}^7F_J$ ($J = 0-4$) f-f transitions of Eu^{3+} ions. The $Eu(III)$ concentration dependence of the photophysical properties was carefully studied. We revealed that Gd-doping results in photoluminescence enhancement due to the heavy atom effect. To quantitatively compare the antenna effect among different compounds, we proposed the new approach, where the quantum yield of the 5D_0 formation is used to characterize the efficiency of energy transfer from the ligand antenna to the Eu^{3+} emitter.

Keywords: metal–organic framework; luminescence; rare earth; europium; yttrium; gadolinium; lanthanum; antenna effect



Citation: Butorlin, O.S.; Petrova, A.S.; Toikka, Y.N.; Kolesnikov, I.E.; Orlov, S.N.; Ryazantsev, M.N.; Bogachev, N.A.; Skripkin, M.Y.; Mereshchenko, A.S. The Structure and Optical Properties of Luminescent Europium Terephthalate Antenna Metal–Organic Frameworks Doped by Yttrium, Gadolinium, and Lanthanum Ions. *Molecules* **2024**, *29*, 3558. <https://doi.org/10.3390/molecules29153558>

Academic Editor: Pierre D. Harvey

Received: 3 July 2024

Revised: 23 July 2024

Accepted: 26 July 2024

Published: 28 July 2024



Copyright: © 2024 by the authors. Licensee MDPI, Basel, Switzerland. This article is an open access article distributed under the terms and conditions of the Creative Commons Attribution (CC BY) license (<https://creativecommons.org/licenses/by/4.0/>).

1. Introduction

Metal–organic frameworks (MOFs) represent a large class of crystalline materials defined as porous networks, consisting of metallic ions or clusters linked together by organic multidentate ligands. Due to their well-defined crystallinity, porosity, high stability, and wide diversity of structures and topologies, these materials have attracted considerable attention in the past two decades. Rare-earth element (REE) metal–organic frameworks (MOFs) are of particular interest due to their unique luminescence properties significantly determined by the type of lanthanide ion. Thus, REE-MOFs have been revealed as promising candidates for light-emitting materials, sensors, multimodal image contrast agents, catalysts, and analytes to reveal the hazardous substances in food and environment [1–7]. The f-f transitions are forbidden by selection rules, which results in inefficiency of direct excitation of lanthanide ions. This problem can be overcome by using the energy transfer from the excited ligand to the lanthanide ion, which is called the “antenna effect” [8,9]. The organic ligands, which are used as “antenna” compounds, have high UV absorption coefficients, easily coordinate with REE ions, and efficiently transfer energy to REE ions. The mechanism of the antenna effect can be explained as follows. Upon photon absorption, the ligand in the ground singlet state (S_0) is promoted to the singlet excited state (S_1, S_2 , etc.), followed by fast internal conversion to a lower excited energy level (S_1). The excited singlet

state can then either (i) return to the ground state ($S_1 \rightarrow S_0$) by internal conversion and fluorescence or (ii) undergo an intersystem crossing to the triplet state. Through internal conversion, the ligand reaches the lowest triplet level electronic state, T_1 , followed by the energy transfer to the REE ion [10]. In Eu-based antenna complexes, the quantum yield of luminescence from the europium ion depends on the relative energy level of the ligand triplet state and the atomic level of the Eu^{3+} ion. Energy transfer has been found to occur from the lowest energy triplet state of the ligand T_1 to the ${}^5\text{D}_J$ ($J = 0-3$) level of the Eu^{3+} ion followed by internal conversion to ${}^5\text{D}_0$. The radiative transitions ${}^5\text{D}_0-{}^7\text{F}_J$ ($J = 0-4$) to the term of ground state ${}^7\text{F}$ of the Eu^{3+} ion correspond to the resulting photoluminescence of such antenna complexes. For the most efficient energy transfer, the difference in energy between the ligand triplet state and the ${}^5\text{D}_J$ level of Eu^{3+} should be approximately $2500-4000 \text{ cm}^{-1}$ [11]. However, it has also been proposed that energy transfer can occur from a singlet excited state as well [12,13]. For example, in a study by Shinji Miyazaki et al., the possibility of two energy transfer pathways was revealed from both the triplet and singlet levels for the $\text{Eu}(\text{hfa})_3(\text{DPPTO})_2$ complex (hfa—hexafluoroacetylacetonate, DPPTO—2-diphenylphosphoryltriphenylene) [14].

The simultaneous presence of both luminescent and nonluminescent REE ions, such as Sc^{3+} , Y^{3+} , La^{3+} , Gd^{3+} , Lu^{3+} , can significantly affect the structural and photophysical properties of these compounds. The structural properties of heterometallic REE-MOFs have been investigated in several studies. It has been found that at low concentrations of the luminescent lanthanide ions, substitution occurs isomorphically, without changing the crystalline structure. However, it has been observed that in some compounds, the structure changes as concentration increases. For example, Jarley Nascimento et al. showed that compounds $\text{Gd}_{1-x}\text{Eu}_x(1,4\text{-bdc})_3(\text{dmf})_2(\text{H}_2\text{O})_n$ (bdc—benzenedicarboxylate, dmf—dimethylformamide; $x = 0.01, 0.03, 0.05, 0.07, 0.09$) are isostructural with $[\text{Eu}_2(1,4\text{-bdc})_3(\text{dmf})_2(\text{H}_2\text{O})]$ at the Eu^{3+} content between 1 and 7 at. % (at. %—the relative atom content of a certain lanthanide to all lanthanide atoms). However, at the Eu^{3+} concentration of 9 at. %, the compound was isostructural with $[\text{Eu}_2(1,4\text{-bdc})_3(\text{dmf})_2(\text{H}_2\text{O})_2]$ [15]. In our previous research, we found that the compound $(\text{Eu}_x\text{Lu}_{1-x})_2(1,4\text{-bdc})_3 \cdot n\text{H}_2\text{O}$ forms different crystal structures depending on the concentration of the Eu^{3+} ions. At the Eu^{3+} concentration range of 6–100 at. %, the samples were found to be isostructural with $\text{Ln}_2(1,4\text{-bdc})_3 \cdot 4\text{H}_2\text{O}$. However at the Eu^{3+} concentration of 0–2 at. %, the samples were isostructural with the Ln_2bdc_3 . At the Eu^{3+} concentration between 3 and 5 at. %, both the $\text{Ln}_2\text{bdc}_3 \cdot 4\text{H}_2\text{O}$ and the $\text{Ln}_2(1,4\text{-bdc})_3$ phases were observed in the samples [16]. The changes in the crystal structure can significantly affect the optical properties of compounds, such as the fine structure of emission spectra, quantum yields, and lifetime values.

Meanwhile, the optical properties of the heterometallic MOFs also depend on the concentration of the luminescent ion in the case of isomorphic substitution of the REE ion by the luminescent ion in the whole concentration range where the single crystalline phase is formed. However, very few works have studied such a concentration dependence. Thus, Utochnikova et al. studied the optical properties of heterometallic solid solutions of $(\text{Tb}_x\text{Y}_{1-x})_2(1,4\text{-bdc})_3(\text{H}_2\text{O})_4$ and $\text{Eu}_x\text{Gd}_{1-x}(\text{dbm})_3(\text{phen})$ (dbm—dibenzoylmethanate, phen—o-phenantroline) MOFs. The steep quantum yield rise was observed at the low concentrations of Eu^{3+} or Tb^{3+} ions. Then, in the range of 20–100 at. % of Tb^{3+} for $(\text{Tb}_x\text{Y}_{1-x})_2(1,4\text{-bdc})_3(\text{H}_2\text{O})_4$ and 10–100 at. % of Eu^{3+} for $\text{Eu}_x\text{Gd}_{1-x}(\text{dbm})_3(\text{phen})$, the quantum yield does not depend on the concentration of the luminescent ions. It has also been observed that lifetimes decrease with increasing concentration of the luminescent ion [17].

We note that the majority of studies focus on compounds with a single or a few concentrations of the luminescent lanthanide ion [17–19] or a narrow range of concentrations [15]. The properties of the synthesized compounds have been studied incompletely, and, therefore, at the moment, we have limited information about the mechanism of the dopant concentration effect on photophysical properties of heterometallic REE-MOFs.

In this article, the photophysical properties (photoluminescence decay time constants, radiative, nonradiative, and total decay rates, quantum efficiencies, and formation quantum

yields of the 5D_0 level; photoluminescence quantum yields, asymmetric ratios) of REE-MOFs of solid solutions of heterometallic $(Eu_xM_{1-x})_2(1,4-bdc)_3 \cdot 4H_2O$ MOFs ($M = Y, La, Gd$) were studied in detail in a wide concentration range of the Eu^{3+} ion (0.1–100 at. %).

2. Results

2.1. Structure and Morphology

The phase composition of $(Eu_xM_{1-x})_2(1,4-bdc)_3 \cdot nH_2O$ ($M = Y, Gd, La$) with a Eu^{3+} concentration from 0 to 100 at. % was studied using powder X-ray diffraction (PXRD). The experimental PXRD patterns at % of the synthesized materials are presented in Figure 1a and Figure S1 (Supplementary Materials). The positions of the diffraction maxima in the PXRD patterns indicate that all the synthesized compounds correspond to the $Ln_2(1,4-bdc)_3 \cdot 4H_2O$ crystalline phase ($Ln = Ce - Yb$) [20], and no additional peaks were observed. In the $Ln_2(1,4-bdc)_3 \cdot 4H_2O$ structure (Figure 1b), the octacoordinated lanthanide ions are bound to the two water molecules and six different terephthalate ions through the oxygen atoms.

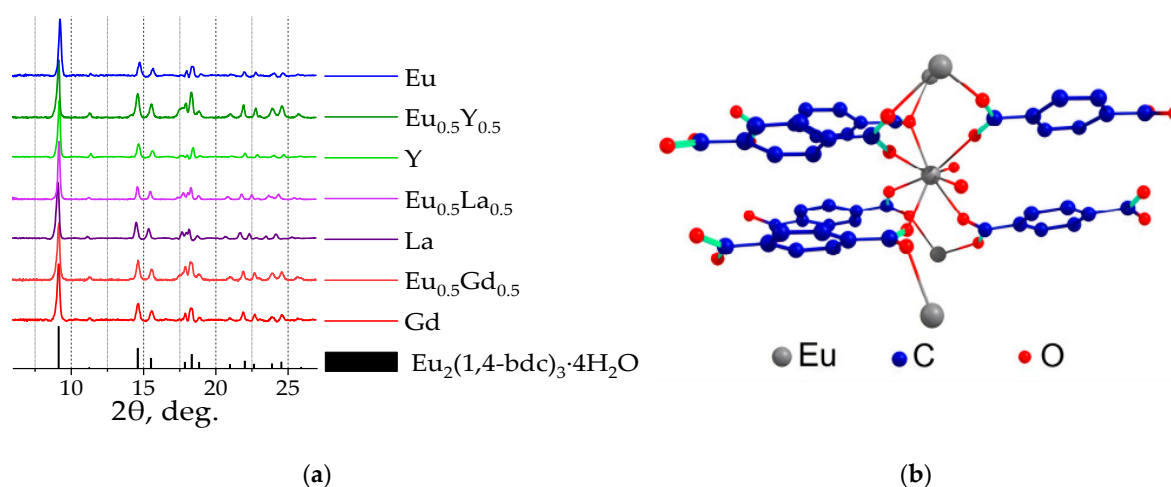


Figure 1. The XRD patterns of selected $(Eu_xM_{1-x})_2bdc_3 \cdot 4H_2O$ ($M = Gd, La, Y; x = 0, 0.5, 1$) and the simulated XRD pattern of $Eu_2(1,4-bdc)_3 \cdot 4H_2O$ single-crystal structure were taken from ref. [20] (a). The crystal structure of $Eu_2(1,4-bdc)_3 \cdot 4H_2O$ (b).

The refinement of the unit cell parameters and the calculation of the unit cell volumes were performed for the selected samples over the Eu^{3+} concentration range between 0 and 100 at. %. Unit cell parameters (Table S1, Supplementary Materials) were refined using UnitCell software [21]. This program can retrieve unit cell parameters from diffraction data using a least-squares method from the positions of the indexed diffraction maxima of the PXRD patterns (Pawley method [22]). The Eu^{3+} concentration effect on the unit cell volumes is shown in Figure 2. For the $(Eu_xLa_{1-x})_2(1,4-bdc)_3 \cdot 4H_2O$ compounds, the increase in La^{3+} content leads to increased unit cell volumes due to a higher ionic radius of La^{3+} ions (1.160 Å, the coordination number is eight) than the ionic radius of Eu^{3+} ions (1.066 Å) [23].

The ionic radius of the Gd^{3+} ion (1.053 Å) is close to that of Eu^{3+} . Therefore, the unit cell parameters do not change significantly in the $(Eu_xGd_{1-x})_2(1,4-bdc)_3 \cdot 4H_2O$ series. The Y^{3+} ion (0.977 Å) is less than Eu^{3+} ; therefore, substitution of Eu^{3+} by the Y^{3+} ion results in a decrease in the unit cell volumes in the $(Eu_xM_{1-x})_2(1,4-bdc)_3 \cdot 4H_2O$ series. In general, the dependence of unit cell volume obeys Vegard's law [24], with a slight deviation from linearity that falls within the error limits.

Scanning electron microscopy (SEM) was used to reveal the particle morphology and the porosity of the selected synthesized materials, namely, $(Eu_{0.5}M_{0.5})_2(1,4-bdc)_3 \cdot 4H_2O$ ($M = Y, La, Gd$). The resulting compounds had a distinct porous structure, as can be seen from the SEM images in Figure 3. On average, the particles are between 5 and 20 μm in size, and the pore diameter ranges from 20 to 150 nanometers. This observation confirms

that the synthesized compounds are MOFs according to the definition of IUPAC [25]. Heterometallic europium terephthalates doped with yttrium and gadolinium formed spindle-shaped particles, while those with lanthanum formed flake-like particles.

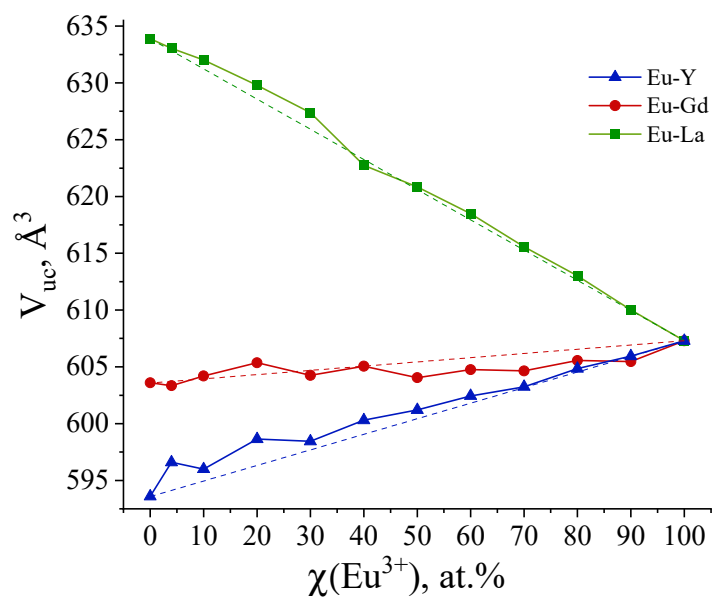


Figure 2. Eu^{3+} concentration dependence of unit cell volume (V_{uc}) refined for $(\text{Eu}_x\text{M}_{1-x})_2(1,4\text{-bdc})_3 \cdot 4\text{H}_2\text{O}$ ($M = \text{Gd}, \text{La}, \text{Y}$).

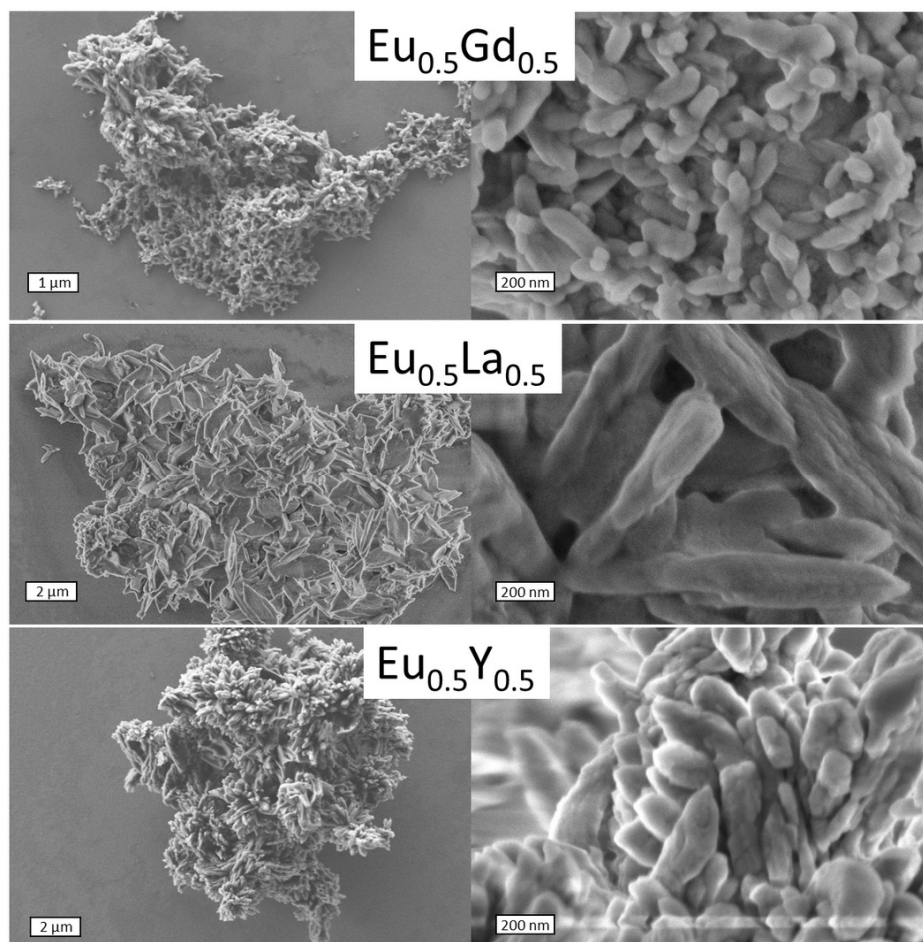


Figure 3. SEM images of $(\text{Eu}_{0.5}\text{M}_{0.5})_2(1,4\text{-bdc})_3 \cdot 4\text{H}_2\text{O}$ ($M = \text{Gd}, \text{La}, \text{Y}$).

2.2. IR Spectroscopy

To reveal the doping effect on the vibrational structure of the ligands, we measured the IR spectra of the selected samples of heterometallic $(\text{Eu}_{0.5}\text{M}_{0.5})_2(1,4\text{-bdc})_3 \cdot 4\text{H}_2\text{O}$ ($\text{M} = \text{Y}, \text{Gd}, \text{La}$) and homometallic $\text{M}_2(1,4\text{-bdc})_3 \cdot 4\text{H}_2\text{O}$ ($\text{M} = \text{Y}, \text{Gd}, \text{La}, \text{Eu}$) terephthalates (Figure 4). The broad band with the maximum at about the 3500 cm^{-1} region corresponds to the O-H stretching vibrations of the water molecules coordinated to the metal. The multiple narrow bands in the $1270\text{--}1470$ and $1470\text{--}1800 \text{ cm}^{-1}$ regions correspond to the symmetric and asymmetric stretching vibrations of the carboxylic $-\text{COO}$ group of the terephthalate ion, respectively. The data obtained are consistent with the data in the literature obtained for REE terephthalates [26,27]. The spectral shape, including the fine structure of the absorption bands and the position of the absorption maxima, is almost identical for the studied compounds, which indicates the similar structure of these terephthalates. This conclusion is in agreement with PXRD data, demonstrating that all the synthesized compounds have the same crystalline phase, namely, $\text{Ln}_2(1,4\text{-bdc})_3 \cdot 4\text{H}_2\text{O}$.

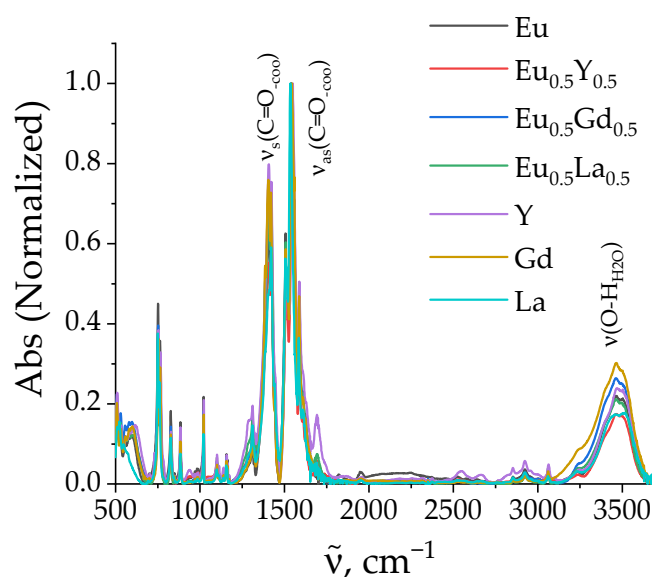


Figure 4. FTIR spectra of $(\text{Eu}_{0.5}\text{M}_{0.5})_2(1,4\text{-bdc})_3 \cdot 4\text{H}_2\text{O}$ ($\text{M} = \text{Y}, \text{Gd}, \text{La}$) and $\text{M}_2(1,4\text{-bdc})_3 \cdot 4\text{H}_2\text{O}$ ($\text{M} = \text{Y}, \text{Gd}, \text{La}, \text{Eu}$).

2.3. Thermogravimetric Analysis

Thermogravimetric analysis (TGA) was performed for selected heterometallic $(\text{Eu}_{0.5}\text{M}_{0.5})_2(1,4\text{-bdc})_3 \cdot 4\text{H}_2\text{O}$ ($\text{M} = \text{Y}, \text{Gd}, \text{La}$) and homometallic $\text{M}_2(1,4\text{-bdc})_3 \cdot 4\text{H}_2\text{O}$ ($\text{M} = \text{Y}, \text{Gd}, \text{La}, \text{Eu}$) terephthalates in the temperature range of $35\text{--}200 \text{ }^\circ\text{C}$ (Figure 5). Weight loss between 8.5 and 9.3% was observed at a temperature of $120\text{--}180 \text{ }^\circ\text{C}$ for all measured samples. As previously reported [28], weight loss in this temperature range may be associated with the dehydration of compounds, leading to the formation of anhydrous terephthalates with a general formula of $\text{M}_2(1,4\text{-bdc})_3$. The weight loss of 8.5–9.3% corresponds to the elimination of 3.8–4.1 water molecules from the initial terephthalates, which is in agreement with the PXRD data, showing that all studied materials are formed in the $\text{Ln}_2(1,4\text{-bdc})_3 \cdot 4\text{H}_2\text{O}$ crystalline phase.

2.4. Luminescent Properties

For all synthesized compounds, emission spectra were measured upon 300 nm excitation into the S_n singlet state of the terephthalate ion. Figure 6 shows the normalized emission spectra of selected samples with different Eu^{3+} content ($(\text{Eu}_x\text{M}_{1-x})_2(1,4\text{-bdc})_3 \cdot 4\text{H}_2\text{O}$ ($\text{M} = \text{Y}, \text{La}, \text{Gd}$) ($x = 0.001, 0.01, 0.1, 0.5, 1$)). The emission spectra of all studied materials are given in Figure S2 (Supplementary Materials). All emission spectra contain the same

narrow bands, which correspond to the $^5D_0-^7F_J$ ($J = 1, 2, 4$) transitions of Eu^{3+} : $^5D_0-^7F_1$ (587.9 and 591.6 nm), $^5D_0-^7F_2$ (614 nm), and $^5D_0-^7F_4$ (696 nm).

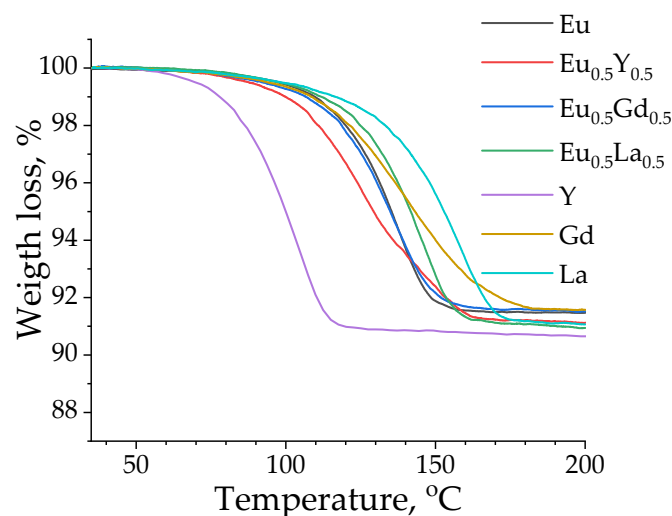


Figure 5. TGA curves of selected heterometallic $(\text{Eu}_{0.5}\text{M}_{0.5})_2(1,4\text{-bdc})_3\cdot 4\text{H}_2\text{O}$ ($\text{M} = \text{Y}, \text{Gd}, \text{La}$) and homometallic $\text{M}_2(1,4\text{-bdc})_3\cdot 4\text{H}_2\text{O}$ ($\text{M} = \text{Y}, \text{Gd}, \text{La}, \text{Eu}$) terephthalates measured in the temperature range of 35–200 °C.

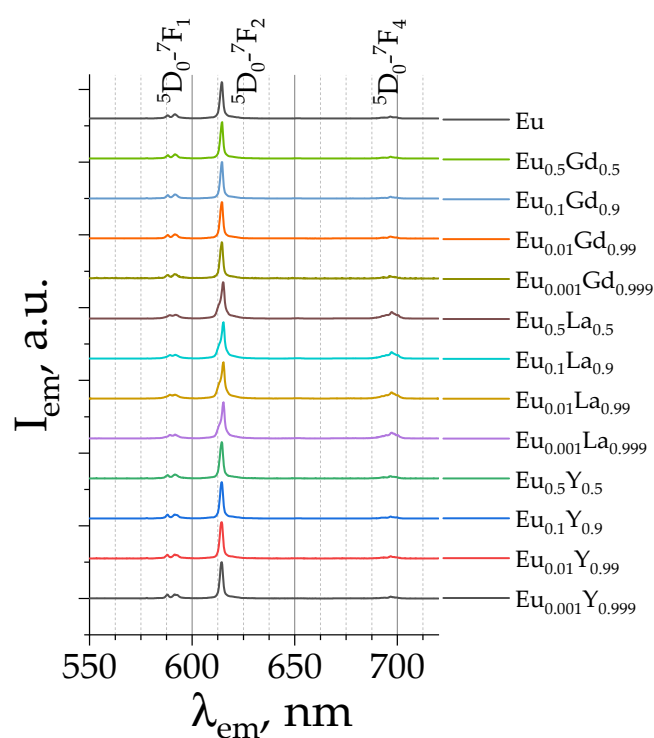


Figure 6. The normalized emission spectra of $(\text{Eu}_x\text{M}_{1-x})_2(1,4\text{-bdc})_3\cdot 4\text{H}_2\text{O}$ ($\text{M} = \text{Gd}, \text{La}, \text{Y}$) at selected Eu^{3+} concentrations (given in legend) upon 300 nm excitation.

$^5D_0-^7F_3$ transitions are also present in emission spectra, but they were not observed due to their weak intensity. The presence of Eu^{3+} f-f bands in the emission spectra upon excitation to the S_n singlet state of the terephthalate ion clearly reveals an antenna effect. Thus, the terephthalate ion absorbs UV radiation followed by efficient energy transfer to the luminescent lanthanide ion. Upon the excitation, the terephthalate ion is promoted into the S_n state, followed by the fast internal conversion to the S_1 state. Due to the heavy atom effect caused by the lanthanide atom, the S_1 state efficiently undergoes intersystem

crossing to the T_1 triplet electronic excited state. The T_1 state of the terephthalate ion is close in energy to the 5D_1 energy level of the Eu^{3+} ion [11,17]. Therefore, an efficient energy transfer occurs from the sensitizer to the luminescent lanthanide ion. The 5D_1 level of Eu^{3+} then undergoes an internal conversion to the 5D_0 state, followed by the emission to the 7F_J ($J = 1, 2, 4$) lower-lying energy levels.

The shape of the emission spectra for the Y-, Gd-, and La-doped compounds is identical to that of the pure europium terephthalate emission spectrum (Figure S3, Supplementary Materials), implying the same coordination environment of Eu^{3+} in the solid solutions studied. This observation agrees with the PXRD data, which show the presence of the same crystalline structure, $(\text{Eu}_x\text{M}_{1-x})_2(1,4\text{-bdc})_3 \cdot 4\text{H}_2\text{O}$ ($\text{M} = \text{Y}, \text{Gd}, \text{La}$), among the studied series. However, the peak intensity of emission spectra depends on the concentrations of europium ions in the studied solid solutions due to different photoluminescence quantum yields, which will be discussed further.

The photoluminescence decay curves of the $(\text{Eu}_x\text{M}_{1-x})_2(1,4\text{-bdc})_3 \cdot 4\text{H}_2\text{O}$ phosphors monitored at 615 nm ($^5D_0 \rightarrow ^7F_2$ transition) are presented in Figure 7 ($\lambda_{\text{ex.}} = 300$ nm). The decay curves were fitted by a single exponential function:

$$I = I_0 \cdot e^{-\frac{t}{\tau}} \quad (1)$$

where τ is the observed 5D_0 lifetime (Table 1).

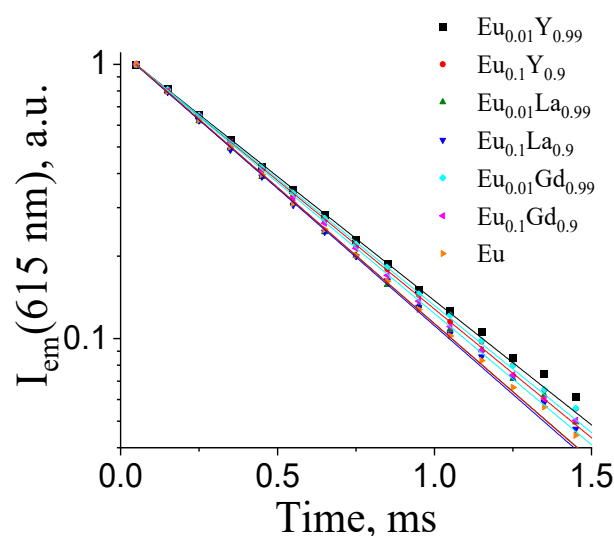


Figure 7. The 615 nm photoluminescence decay curves of $(\text{Eu}_x\text{M}_{1-x})_2(1,4\text{-bdc})_3 \cdot 4\text{H}_2\text{O}$ ($\text{M} = \text{Y}, \text{La}, \text{Gd}$; $x = 0.01, 0.1$).

Table 1. The observed 5D_0 lifetime of $(\text{Eu}_x\text{M}_{1-x})_2(1,4\text{-bdc})_3 \cdot 4\text{H}_2\text{O}$ ($\text{M} = \text{Gd}, \text{La}, \text{Y}$; $x = 0.01, 0.1$).

$\text{Eu}_x\text{M}_{1-x}$	$\tau(^5D_0)$, ms
$\text{Eu}_{0.01}\text{Gd}_{0.99}$	0.48 ± 0.01
$\text{Eu}_{0.1}\text{Gd}_{0.9}$	0.46 ± 0.01
$\text{Eu}_{0.01}\text{La}_{0.99}$	0.44 ± 0.01
$\text{Eu}_{0.1}\text{La}_{0.9}$	0.43 ± 0.01
$\text{Eu}_{0.01}\text{Y}_{0.99}$	0.47 ± 0.01
$\text{Eu}_{0.1}\text{Y}_{0.9}$	0.45 ± 0.01
Eu	0.44 ± 0.01

Figure 7 and Table 1 present the photoluminescence decay curves and lifetime data for the selected concentrations of Eu^{3+} ions in $(\text{Eu}_x\text{M}_{1-x})_2(1,4\text{-bdc})_3 \cdot 4\text{H}_2\text{O}$ ($\text{M} = \text{Gd}, \text{La}, \text{Y}$) ($x = 0.01, 0.1$, and 1) among the whole concentration range. As can be seen from Table 1, all the samples have similar lifetimes. This allows us to assume that the 5D_0 lifetime of

the Eu^{3+} ion almost does not depend on the Eu^{3+} content in the 1–100 at. % concentration range of Eu^{3+} .

The measured photoluminescence quantum yields (PLQYs) of the $(\text{Eu}_x\text{M}_{1-x})_2(1,4\text{-bdc})_3\cdot 4\text{H}_2\text{O}$ are shown in Figure 8a. It should be noted that the ${}^5\text{D}_0$ lifetimes do not depend significantly on the sample composition and are equal to about 0.45 ms. Meanwhile, the photoluminescence luminescence quantum yields increase with an increase in the Eu^{3+} concentration from 1 to 10 at. % due to the number of luminescence sites increasing. In particular, for the Eu–Y series, there is a rapid increase in the quantum yield up to 10%, after which the PLQY remains within small deviations of values from 10 at. % and reaches a plateau, up to Eu 100%. For the Eu–La series, there is also a rapid increase in the PLQY at low concentrations of Eu up to ~12% and a slight decrease in quantum yield to 10% in the range of Eu concentrations from 20 to 100 at. %. The Eu–Gd series is different from the Eu–Y and Eu–La ones: the PLQY has a maximum at the Eu^{3+} content of 10 at. %. The PLQY of $(\text{Eu}_{0.1}\text{Gd}_{0.9})_2(1,4\text{-bdc})_3\cdot 4\text{H}_2\text{O}$ is equal to 15%, which is 1.5 times greater than that of $(\text{Eu}_{0.1}\text{Y}_{0.9})_2(1,4\text{-bdc})_3\cdot 4\text{H}_2\text{O}$ and $(\text{Eu}_{0.1}\text{La}_{0.9})_2(1,4\text{-bdc})_3\cdot 4\text{H}_2\text{O}$. Upon further Eu^{3+} content increase, the PLQY of $(\text{Eu}_x\text{Gd}_{1-x})_2(1,4\text{-bdc})_3\cdot 4\text{H}_2\text{O}$ decreases, whereas the PLQY of $(\text{Eu}_x\text{Y}_{1-x})_2(1,4\text{-bdc})_3\cdot 4\text{H}_2\text{O}$ and $(\text{Eu}_x\text{La}_{1-x})_2(1,4\text{-bdc})_3\cdot 4\text{H}_2\text{O}$ stays about the same (10%).

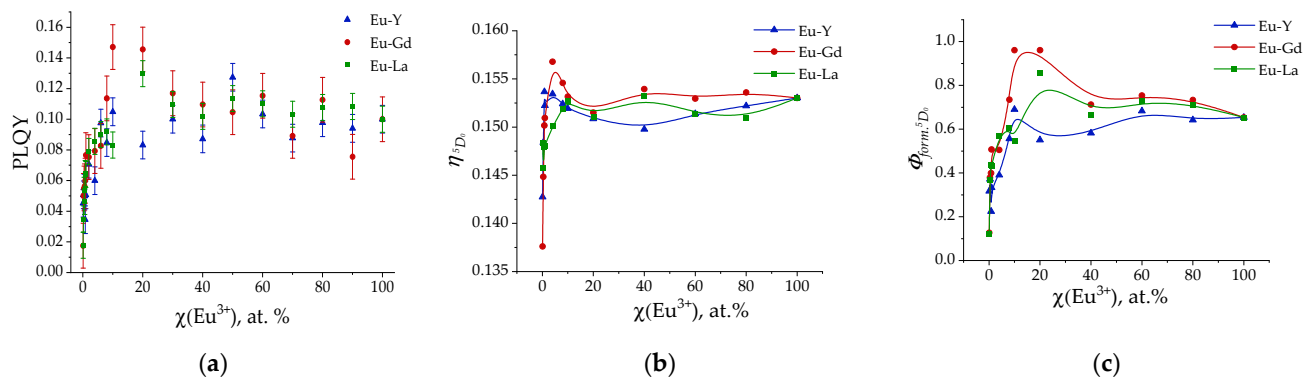


Figure 8. Photoluminescence quantum yield (PLQY) (a), quantum efficiency (η) ${}^5\text{D}_0$ of Eu^{3+} (b), and quantum yield of ${}^5\text{D}_0$ formation (c) of $(\text{Eu}_x\text{M}_{1-x})_2(1,4\text{-bdc})_3\cdot 4\text{H}_2\text{O}$ ($\text{M} = \text{Gd}, \text{La}, \text{Y}$).

Luminescence decay is determined by both radiative and nonradiative processes. Radiative decay rate is determined by dipole transition strength and local-field correction. Nonradiative processes include multiphonon relaxation, quenching on impurities, and cooperative processes such as cross-relaxation and energy migration, the influence of which increases with increasing concentration of europium ions in the solid solution. Radiative and nonradiative decay rates of Eu^{3+} -doped phosphors can be calculated from the emission spectrum using the 4f–4f intensity theory [29]. The magnetic dipole ${}^5\text{D}_0\text{--}{}^7\text{F}_1$ transition probability $A_{0-1} = A_{MD0} \cdot n_0^3 = 49 \text{ s}^{-1}$. A_{MD0} is the spontaneous emission probability of the magnetic dipole ${}^5\text{D}_0\text{--}{}^7\text{F}_1$, 14.65 s^{-1} , and n_0 is the refractive index, 1.5 [30]. Radiative decay rates A_{0-J} ($J = 2, 4$) of the ${}^5\text{D}_0\text{--}{}^7\text{F}_J$ emission transition can be obtained as follows:

$$A_{0-J} = A_{0-1} \cdot \frac{\nu_{0-1} \cdot I_{0-J}}{\nu_{0-J} \cdot I_{0-1}} \quad (2)$$

where ν_{0-J} and I_{0-J} are, respectively, the frequency and intensity of the corresponding transition ${}^5\text{D}_0\text{--}{}^7\text{F}_J$ in the emission spectrum. The radiative decay rate is the sum of all the A_{0-J} values $A_{Rad} = A_{0-1} + A_{0-2} + A_{0-4}$. The nonradiative decay rate can be determined using the observed lifetime and the obtained radiative decay rate: $A_{total} = A_{Rad} + A_{Nonrad} = \frac{1}{\tau_f}$; the quantum efficiency of the ${}^5\text{D}_0$ is

$$\eta_{{}^5\text{D}_0} = \frac{A_{Rad}}{A_{total}} = \frac{n({}^5\text{D}_0\text{--}{}^7\text{F}_J)_{em.}}{n({}^5\text{D}_0)} \quad (3)$$

Knowledge of both the PLQY (Figure 8a) and the quantum efficiency of 5D_0 (Figure 8b) allows us to calculate the quantum yield of the 5D_0 formation. The studied terephthalate solid solutions are antenna complexes, where 5D_0 is populated as a result of the energy transfer from the initial excited terephthalate ion ($S_n(\text{bdc}^{2-}) \rightarrow S_1(\text{bdc}^{2-}) \rightarrow T_1(\text{bdc}^{2-}) \rightarrow {}^5D_0(\text{Eu}^{3+})$). Therefore, the PLQY can be calculated as the direct product of the quantum efficiency of the 5D_0 ($\eta_{{}^5D_0}$) and quantum yield of the 5D_0 formation ($\Phi_{\text{form.}{}^5D_0}$):

$$\text{PLQY} = \eta_{{}^5D_0} \cdot \Phi_{\text{form.}{}^5D_0} \quad (4)$$

Therefore, the quantum yield of the 5D_0 formation (Figure 8c) was calculated as follows:

$$\Phi_{\text{form.}{}^5D_0} = \frac{\text{PLQY}}{\eta_{{}^5D_0}} \quad (5)$$

At Eu^{3+} concentrations up to 10 at. %, the quantum yield of the 5D_0 formation increases as a result of the number of luminescence sites increasing. For the Eu–Y series, it remains unchanged up to 100 at. % of Eu^{3+} , whereas for the Eu–La and Eu–Gd series, it reaches a maximum at 10 at. % of Eu^{3+} and then decays. The maximum values of quantum yield of the 5D_0 formation decrease in a dopant row of Gd–La–Y. The QY of 5D_0 formation is close to 100%, which indicates a very-high-efficiency energy transfer from the terephthalate antenna to the light-emitting Eu^{3+} ion. We propose that this observation can be explained by the heavy atom effect, which is more pronounced for the Gd^{3+} ion and less pronounced for the Y^{3+} ion.

The emission spectrum of the Eu^{3+} ion includes a very sensitive forced electric dipole transition ${}^5D_0 \rightarrow {}^7F_2$. At the same time, the ${}^5D_0 \rightarrow {}^7F_1$ magnetic dipole transition is not sensitive to environmental changes. Changes in the environment can be judged by the asymmetry ratio, which is determined by the ratio between the ${}^5D_0 \rightarrow {}^7F_2$ and ${}^5D_0 \rightarrow {}^7F_1$ transition intensities. The higher the asymmetry coefficient, the further away the luminescence center is located from the centrosymmetric geometry [31]. The effect of Eu^{3+} ion concentration on local symmetry in samples $(\text{Eu}_x\text{M}_{1-x})_2(1,4\text{-bdc})_3 \cdot 4\text{H}_2\text{O}$ MOFs ($\text{M} = \text{Y}, \text{La}, \text{Gd}$) is shown in Figure 9. It is seen that an increase in the concentration of the Eu^{3+} ion leads to the growth of the asymmetry ratio due to distortion of the crystal structure near the luminescent atom. Starting from 10 at. % of Eu^{3+} , the asymmetry ratio reaches a plateau and does not change within the margin of error. Thus, the data once again confirm the fact that three-charged REE ions replace each other isomorphically in crystalline substances.

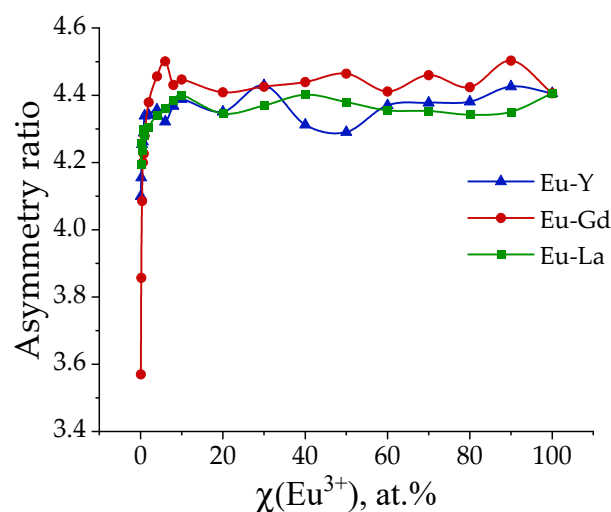


Figure 9. Asymmetric ratios of $(\text{Eu}_x\text{M}_{1-x})_2(1,4\text{-bdc})_3 \cdot 4\text{H}_2\text{O}$ ($\text{M} = \text{Gd}, \text{La}, \text{Y}$).

The abovementioned results clearly show that the presence of a gadolinium ion leads to the luminescence enhancement in Eu–Gd terephthalates, whereas this effect is

almost not pronounced in the Eu–La and Eu–Y series. Thus, $(\text{Eu}_{0.1}\text{Gd}_{0.9})_2(1,4\text{-bdc})_3\cdot 4\text{H}_2\text{O}$ demonstrates the maximum PLQY among the Eu–Gd series, 15%. The PLQY value is 4–5% higher than that in the Eu–La and Eu–Y series at the same Eu^{3+} ion content (10 at. %). At the higher Eu^{3+} concentrations, the values of PLQY decrease smoothly for the Eu–Gd series, reaching 10% for $\text{Eu}_2(1,4\text{-bdc})_3\cdot 4\text{H}_2\text{O}$. For the Eu–La and Eu–Y series, the PLQY stays about the same (9–11%) up to Eu^{3+} concentration of 100 at. %. Therefore, we do not observe Eu^{3+} concentration quenching. The Gd-doping effect is also observed for the calculated values of ${}^5\text{D}_0$ formation quantum yield: for $(\text{Eu}_{0.1}\text{Gd}_{0.9})_2(1,4\text{-bdc})_3\cdot 4\text{H}_2\text{O}$, the QY of ${}^5\text{D}_0$ formation values become close to 100%, which indicates a very-high-efficiency energy transfer from the terephthalate antenna to the light-emitting Eu^{3+} ion. The Gd^{3+} ion has an f^7 configuration and, therefore, increases the probability (rate) of $\text{S}_1\text{-T}_1$ intersystem crossing in the terephthalate ion, which is associated with the heavy atom effect manifested by paramagnetic Gd^{3+} ions. To confirm the proposed mechanism, we measured the emission spectra of gadolinium and yttrium terephthalates upon 300 nm excitation into the ${}^1\pi\pi$ band of the terephthalate ion. The prominent increase in the phosphorescence band (510 nm) was observed for $\text{Gd}_2(1,4\text{-bdc})_3\cdot 4\text{H}_2\text{O}$ compared with $\text{Y}_2(1,4\text{-bdc})_3\cdot 4\text{H}_2\text{O}$, which confirms the increase in the intersystem crossing quantum yield resulting from the increase in the $\text{S}_1\text{-T}_1$ nonradiative transition rate (Figure 10) as a result of the presence of the Gd^{3+} ion.

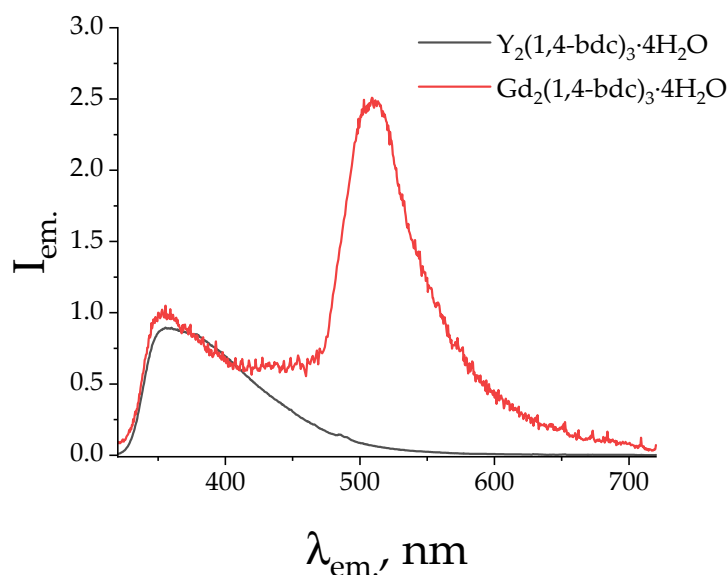


Figure 10. The emission spectra of $\text{Gd}_2(1,4\text{-bdc})_3\cdot 4\text{H}_2\text{O}$ and $\text{Y}_2(1,4\text{-bdc})_3\cdot 4\text{H}_2\text{O}$ upon 300 nm excitation.

3. Materials and Methods

Europium (III) chloride hexahydrate, yttrium (III) chloride hexahydrate, gadolinium (III) chloride hexahydrate, and lanthanum (III) chloride hexahydrate were purchased from Chemcraft (Kaliningrad, Russia). Benzene-1,4-dicarboxylic (terephthalic, $\text{H}_2(1,4\text{-bdc})$) acid (>98%), sodium hydroxide (>99%), nickel(II) chloride hexahydrate (>99%), EDTA disodium salt (0.1 M aqueous solution), and murexide were purchased from Sigma-Aldrich Chemie GmbH (Taufkirchen, Germany) and used without additional purification.

The 0.2 M solutions of EuCl_3 , YCl_3 , GdCl_3 , and LaCl_3 were prepared and standardized using back complexometric titration with EDTA and nickel chloride solution in the presence of an ammonia buffer (pH \approx 9). A total of 0.6 mole of sodium hydroxide and 0.3 mole of terephthalic acid were dissolved in distilled water to obtain a 1 L solution of a 0.3 M solution of the disodium terephthalate ($\text{Na}_2(1,4\text{-bdc})$).

Heterometallic terephthalates with a general formula $(\text{Eu}_x\text{M}_{1-x})_2(1,4\text{-bdc})_3\cdot 4\text{H}_2\text{O}$ ($\text{M} = \text{Y}, \text{Gd}, \text{La}$) were obtained by mixing 0.2 M EuCl_3 , 0.2 M MCl_3 ($\text{M} = \text{Y}, \text{La}, \text{Gd}$) with 2 mL of 0.3 M Na_2bdc water solution. EuCl_3 and MCl_3 were taken in stoichiometric ratios.

The total volume of 0.2 M EuCl_3 and 0.2 M MCl_3 solutions was equal to 1 mL. White precipitates of the resulting terephthalates were separated from the reaction mixture using centrifugation ($4000\times g$) and washed using deionized water 3 times. The samples of compounds were then dried at 60°C .

The $\text{Eu}^{3+}/\text{M}^{3+}$ ($\text{M} = \text{Y, Gd, La}$) ratios in the heterometallic terephthalates were confirmed using energy-dispersive X-ray spectroscopy (EDX) (EDX spectrometer EDX-800P, Shimadzu, Kyoto, Japan). The Eu/M ($\text{M} = \text{Y, Gd, La}$) ratios obtained from EDX were consistent with the expected ratios of $\text{Eu}^{3+}/\text{M}^{3+}$ ($\text{M} = \text{Y, Gd, La}$) taken for the synthesis for Eu^{3+} content within 1 at. % accuracy for the most of the samples. The EDX data are provided in the Supplementary Materials in Table S2. X-ray powder diffraction (PXRD) measurements were performed with a D2 Phaser (Bruker, Billerica, MA, USA) X-ray diffractometer using $\text{Cu K}\alpha$ radiation ($\lambda = 1.54056 \text{ \AA}$). Thermogravimetry curves were obtained using a TG 209 F1 Libra thermo-microbalance (Netzsch, Selb, Germany). The measurement of FTIR spectra was carried out using the IRAffinity-1 spectrometer (Shimadzu, Kyoto, Japan). To carry out photoluminescence studies, the synthesized samples (20 mg) and potassium bromide (300 mg) were pressed into pellets (diameter 13 mm). The photoluminescence data were obtained with a Fluoromax-4 fluorescence spectrometer (Horiba Jobin Yvon, Kyoto, Japan). Lifetime measurements were performed with the same spectrometer using a pulsed Xe lamp (pulse duration: 3 μs). The absolute values of the photoluminescence quantum yields were recorded using a Fluorolog 3 Quanta-phi device (Horiba Jobin Yvon, Kyoto, Japan). All measurements were performed at 25°C .

4. Conclusions

In this study, we explored the structure and the optical properties of brightly luminescent heterometallic terephthalate antenna MOFs, namely, $(\text{Eu}_x\text{M}_{1-x})_2(1,4\text{-bdc})_3\cdot 4\text{H}_2\text{O}$ ($\text{M} = \text{Y, La, Gd}$) ($x = 0.001\text{--}1$), which were obtained by precipitation from the aqueous solutions. The crystalline phase of all synthesized compounds corresponds to the $\text{Ln}_2(1,4\text{-bdc})_3\cdot 4\text{H}_2\text{O}$ ($\text{Ln} = \text{Ce} - \text{Yb}$) [20]. Unit cell parameters of the obtained compounds were refined by Pawley method. The replacement of Eu^{3+} ions by the larger La^{3+} ions results in an increase in unit cell parameters in $(\text{Eu}_x\text{La}_{1-x})_2(1,4\text{-bdc})_3\cdot 4\text{H}_2\text{O}$ compounds, whereas the substitution of Eu^{3+} by smaller Y^{3+} ion results in a decrease in the unit cell volumes in the $(\text{Eu}_x\text{M}_{1-x})_2(1,4\text{-bdc})_3\cdot 4\text{H}_2\text{O}$ series. Unit cell parameters almost do not change in the $(\text{Eu}_x\text{Gd}_{1-x})_2(1,4\text{-bdc})_3\cdot 4\text{H}_2\text{O}$ series due to close values of ionic radii of Eu^{3+} and Gd^{3+} . The dependence of unit cell volume obeys Vegard's law [24], which allows one to consider the studied systems as solid solutions. All compounds demonstrate a pronounced antenna effect. Upon 300 nm excitation into S_n singlet state of the terephthalate ion, obtained compounds demonstrate emission corresponding to the ${}^5\text{D}_0\text{--}{}^7\text{F}_j$ ($j = 1, 2, 4$) transitions of Eu^{3+} : ${}^5\text{D}_0\text{--}{}^7\text{F}_1$ (587.9 and 591.6 nm), ${}^5\text{D}_0\text{--}{}^7\text{F}_2$ (614 nm, maximal intensity), and ${}^5\text{D}_0\text{--}{}^7\text{F}_4$ (696 nm). The shape of the emission spectra for the Y-, Gd-, and La-doped compounds is identical to that of pure europium terephthalate emission spectrum due to same local symmetry of Eu^{3+} in the studied solid solutions as a result of crystalline phase isomorphism. The ${}^5\text{D}_0$ excited state lifetime does not depend on the sample composition and is equal to 0.45 ± 0.03 ms. Meanwhile, the peak intensity of emission spectra depends on the concentrations of europium ions in the studied solid solutions due to different photoluminescence quantum yields. Thus, the peak emission intensities and photoluminescence quantum yields increase with an increase in the Eu^{3+} concentration from 1 to 10 at. % due to the number of luminescence sites increasing. At larger Eu^{3+} concentrations, for the Eu–Y and Eu–La series, PLQY and the peak emission intensities remain the same (about 9–11%), whereas in the Eu–Gd series, they reach a maximum of 15% at the Eu^{3+} content of 10 at. % and then slightly decrease, reaching 10% in pure europium(III) terephthalate. The quantum efficiency of the ${}^5\text{D}_0$ state was calculated using the relative intensities of ${}^5\text{D}_0\text{--}{}^7\text{F}_j$ ($j = 1, 2, 4$) transitions and ${}^5\text{D}_0$ excited state lifetimes. To quantitatively compare the antenna effect among different compounds, we propose to use the new approach. Based on the values of PLQYs and quantum efficiency of the ${}^5\text{D}_0$ state, we calculated the quantum yields of the

5D_0 formation, which reflect the efficiency of energy transfer from the ligand antenna to the Eu^{3+} emitter. The quantum yields of 5D_0 formation are larger for Gd^{3+} -doped terephthalates. In the MOFs possessing the highest reported compound values of the PLQY, namely, $(Eu_{0.1}Gd_{0.9})_2(1,4-bdc)_3 \cdot 4H_2O$, the value of quantum yield of 5D_0 formation is close to 100%, which indicates a very high efficiency of the energy transfer from the terephthalate antenna to the light-emitting Eu^{3+} ion. The Gd^{3+} ion has the f^7 configuration and, therefore, the increase in the probability (rate) of S_1-T_1 intersystem crossing in the terephthalate ion is associated with the heavy atom effect of paramagnetic Gd^{3+} ions, resulting in the increase in emission intensity, PLQY, and quantum yields of 5D_0 formation.

Supplementary Materials: The following supporting information can be downloaded at: <https://www.mdpi.com/article/10.3390/molecules29153558/s1>, Figure S1: The powder X-ray diffraction (PXRD) patterns of the synthesized compounds series: (a) $(Eu_xGd_{1-x})_2(1,4-bdc)_3 \cdot nH_2O$ ($x = 0.001-1$) including the $Gd_2(1,4-bdc)_3 \cdot nH_2O$, (b) $(Eu_xLa_{1-x})_2(1,4-bdc)_3 \cdot nH_2O$ ($x = 0.001-1$) including the $La_2(1,4-bdc)_3 \cdot nH_2O$, (c) $(Eu_xY_{1-x})_2(1,4-bdc)_3 \cdot nH_2O$ ($x = 0.001-1$) including the $Y_2(1,4-bdc)_3 \cdot nH_2O$. The positions and relative intensities of diffraction maxima of $Eu_2(1,4-bdc)_3 \cdot 4H_2O$ taken from ref. [20] are shown as bars, Figure S2: The normalized emission spectra of (a) $(Eu_xGd_{1-x})_2(1,4-bdc)_3 \cdot 4H_2O$, (b) $(Eu_xLa_{1-x})_2(1,4-bdc)_3 \cdot 4H_2O$, and (c) $(Eu_xY_{1-x})_2(1,4-bdc)_3 \cdot 4H_2O$ at a wide concentration range of Eu^{3+} ($x = 0.001-1$; given in legend) upon 300 nm excitation, Figure S3: The superimposed emission spectra of (a) $(Eu_xGd_{1-x})_2(1,4-bdc)_3 \cdot 4H_2O$, (b) $(Eu_xLa_{1-x})_2(1,4-bdc)_3 \cdot 4H_2O$, and (c) $(Eu_xY_{1-x})_2(1,4-bdc)_3 \cdot 4H_2O$ at a wide concentration range of Eu^{3+} ($x = 0.001-1$; given in legend) upon 300 nm excitation, Table S1: Unit cell parameters of the $(Eu_xM_{1-x})_2(1,4-bdc)_3 \cdot 4H_2O$ ($M = Y, La, Gd$; $x = 0.04-1$). Table S2: Eu^{3+} atomic fractions (at. %) in the synthesized compounds, namely, $(Eu_xM_{1-x})_2(1,4-bdc)_3 \cdot 4H_2O$. Measured data were obtained from EDX.

Author Contributions: Conceptualization, A.S.M., A.S.P. and O.S.B.; methodology, A.S.M., Y.N.T., A.S.P. and O.S.B.; validation, M.N.R. and I.E.K.; formal analysis, A.S.M., A.S.P. and O.S.B.; investigation, A.S.M., A.S.P., S.N.O., I.E.K. and O.S.B.; resources, A.S.M., M.Y.S. and N.A.B.; data curation, A.S.M., A.S.P. and O.S.B.; writing—original draft preparation, A.S.M., N.A.B., A.S.P. and O.S.B.; writing—review and editing, M.Y.S., Y.N.T., I.E.K., N.A.B., A.S.P., O.S.B. and A.S.M.; visualization, A.S.M., A.S.P. and O.S.B.; supervision, A.S.M.; project administration, A.S.M.; funding acquisition, A.S.M. All authors have read and agreed to the published version of the manuscript.

Funding: This work was supported by the Russian Science Foundation under grant No. 22-73-10040 (<https://rscf.ru/en/project/22-73-10040/>, accessed on 2 July 2024).

Institutional Review Board Statement: Not applicable.

Informed Consent Statement: Not applicable.

Data Availability Statement: The original contributions presented in the study are included in the article (and Supplementary Material), further inquiries can be directed to the corresponding authors.

Acknowledgments: The measurements were performed in the Research Park of Saint Petersburg State University (Magnetic Resonance Research Centre, Chemical Analysis and Materials Research Centre, Cryogenic Department, Interdisciplinary Resource Centre for Nanotechnology, Centre for X-ray Diffraction Studies, Centre for Optical and Laser Materials Research, Thermogravimetric and Calorimetric Research Centre, and Centre for Innovative Technologies of Composite Nanomaterials). This article was published in commemoration of the 300th anniversary of Saint Petersburg State University's founding.

Conflicts of Interest: The authors declare no conflicts of interest.

References

1. Cui, Y.; Chen, B.; Qian, G. Lanthanide metal-organic frameworks for luminescent sensing and light-emitting applications. *Coord. Chem. Rev.* **2014**, *273*, 76–86. [[CrossRef](#)]
2. Chen, B.; Wang, L.; Xiao, Y.; Fronczek, F.R.; Xue, M.; Cui, Y.; Qian, G. A luminescent metal-organic framework with lewis basic pyridyl sites for the sensing of metal ions. *Angew. Chem. Int. Ed.* **2009**, *48*, 500–503. [[CrossRef](#)] [[PubMed](#)]
3. Harbuzaru, B.V.; Corma, A.; Rey, F.; Atienzar, P.; Jorda, J.L.; García, H.; Rocha, J. Metal-organic nanoporous structures with anisotropic photoluminescence and magnetic properties and their use as sensors. *Angew. Chem. Int. Ed.* **2008**, *47*, 1080–1083. [[CrossRef](#)] [[PubMed](#)]

4. Pellé, F.; Aschehoug, P.; Surblé, S.; Millange, F.; Serre, C.; Férey, G. Interactions between Eu^{3+} ions in inorganic–organic hybrid materials. *J. Solid State Chem.* **2010**, *183*, 795–802. [[CrossRef](#)]
5. Lee, J.; Farha, O.K.; Roberts, J.; Scheidt, K.A.; Nguyen, S.T.; Hupp, J.T. Metal-organic framework materials as catalysts. *Chem. Soc. Rev.* **2009**, *38*, 1450–1459. [[CrossRef](#)] [[PubMed](#)]
6. Massi, M.; Ogden, M. Luminescent lanthanoid calixarene complexes and materials. *Materials* **2017**, *10*, 1369. [[CrossRef](#)] [[PubMed](#)]
7. Alpha, B.; Ballardini, R.; Balzani, V.; Lehn, J.; Perathoner, S.; Sabbatini, N. Antenna effect in luminescent lanthanide cryptates: A photophysical study. *Photochem. Photobiol.* **1990**, *52*, 299–306. [[CrossRef](#)]
8. Zhang, X.; Huang, T.; Gao, Y.; Cai, Y.; Liu, J.; Ramachandriah, K.; Mao, J.; Ke, F. Functional modification engineering of metal–organic frameworks for the contaminants detection in food. *Coord. Chem. Rev.* **2024**, *516*, 215990. [[CrossRef](#)]
9. Tan, G.; Wang, S.; Yu, J.; Chen, J.; Liao, D.; Liu, M.; Nezamzadeh-Ejhieh, A.; Pan, Y.; Liu, J. Detection mechanism and the outlook of metal-organic frameworks for the detection of hazardous substances in milk. *Food Chem.* **2024**, *430*, 136934. [[CrossRef](#)]
10. Cao, W.; Tang, Y.; Cui, Y.; Qian, G. Energy transfer in metal–organic frameworks and its applications. *Small Struct.* **2020**, *1*, 2000019. [[CrossRef](#)]
11. Latva, M.; Takalo, H.; Mikkala, V.-M.; Matachescu, C.; Rodriguez-Ubis, J.C.; Kankare, J. Correlation between the lowest triplet state energy level of the ligand and lanthanide(III) luminescence quantum yield. *J. Lumin.* **1997**, *75*, 149–169. [[CrossRef](#)]
12. Yang, C.; Fu, L.M.; Wang, Y.; Zhang, J.P.; Wong, W.T.; Ai, X.C.; Qiao, Y.F.; Zou, B.S.; Gui, L.L. A highly luminescent europium complex showing visible-light-sensitized red emission: Direct observation of the singlet pathway. *Angew. Chem. Int. Ed.* **2004**, *116*, 5119. [[CrossRef](#)]
13. Kasprzycka, E.; Trush, V.A.; Amirkhanov, V.M.; Jerzykiewicz, L.; Malta, O.L.; Legendziewicz, J.; Gawryszewska, P. Contribution of energy transfer from the singlet state to the sensitization of Eu^{3+} and Tb^{3+} luminescence by sulfonylamidophosphates. *Chem.—Eur. J.* **2017**, *23*, 1318–1330. [[CrossRef](#)] [[PubMed](#)]
14. Miyazaki, S.; Miyata, K.; Sakamoto, H.; Suzue, F.; Kitagawa, Y.; Hasegawa, Y.; Onda, K. Dual energy transfer pathways from an antenna ligand to lanthanide ion in trivalent europium complexes with phosphine oxide bridges. *J. Phys. Chem. A* **2020**, *124*, 6601–6606. [[CrossRef](#)] [[PubMed](#)]
15. Do Nascimento, J.F.S.; de Araujo, A.M.U.; Kulesza, J.; de Farias Monteiro, A.F.; Ju´nior, S.A.; Barros, B.S. Solid-state tunable photoluminescence in gadolinium-organic frameworks: Effect of the Eu^{3+} content and co-doping with Tb^{3+} . *New J. Chem.* **2018**, *42*, 5514–5522. [[CrossRef](#)]
16. Nosov, V.G.; Kupryakov, A.S.; Kolesnikov, I.E.; Vidyakina, A.A.; Tumkin, I.I.; Kolesnik, S.S.; Ryazantsev, M.N.; Bogachev, N.A.; Skripkin, M.Y.; Mereshchenko, A.S. Heterometallic Europium(III)–lutetium(III) terephthalates as bright luminescent antenna MOFs. *Molecules* **2022**, *27*, 5763. [[CrossRef](#)] [[PubMed](#)]
17. Utochnikova, V.V.; Grishko, A.Y.; Koshelev, D.S.; Averin, A.A.; Lepnev, L.S.; Kuzmina, N.P. Lanthanide heterometallic terephthalates: Concentration quenching and the principles of the “multiphotonic emission”. *Opt. Mater.* **2017**, *74*, 201–208. [[CrossRef](#)]
18. Alammari, T.; Hlova, I.Z.; Gupta, S.; Biswas, A.; Ma, T.; Zhou, L.; Balema, V.; Pecharsky, V.K.; Mudring, A.-V. Mechanochemical synthesis, luminescent and magnetic properties of lanthanide benzene-1,4-dicarboxylate coordination polymers $(\text{Ln}_{0.5}\text{Gd}_{0.5})_2(1,4\text{-BDC})_3(\text{H}_2\text{O})_4$; Ln = Sm, Eu, Tb. *New J. Chem.* **2020**, *44*, 1054–1062. [[CrossRef](#)]
19. Do Nascimento, J.F.S.; Barros, B.S.; Kulesza, J.; de Oliveira, J.B.L.; Pereira Leite, A.K.; de Oliveira, R.S. Influence of synthesis time on the microstructure and photophysical properties of Gd-MOFs doped with Eu^{3+} . *Mater. Chem. Phys.* **2017**, *190*, 166–174. [[CrossRef](#)]
20. Reineke, T.M.; Eddaoudi, M.; Fehr, M.; Kelley, D.; Yaghi, O.M. From condensed lanthanide coordination solids to microporous frameworks having accessible metal sites. *J. Am. Chem. Soc.* **1999**, *121*, 1651–1657. [[CrossRef](#)]
21. Holland, T.J.B.; Redfern, S.A.T. Unit cell refinement from powder diffraction data: The use of regression diagnostics. *Mineral. Mag.* **1997**, *61*, 65–77. [[CrossRef](#)]
22. Pawley, G.S. Unit-cell refinement from powder diffraction scans. *J. Appl. Crystallogr.* **1981**, *14*, 357–361. [[CrossRef](#)]
23. Shannon, R.D. Revised effective ionic radii and systematic studies of interatomic distances in halides and chalcogenides. *Acta Crystallogr. Sect. A* **1976**, *32*, 751–767. [[CrossRef](#)]
24. Denton, A.R.; Ashcroft, N.W. Vegard’s law. *Phys. Rev. A* **1991**, *43*, 3161. [[CrossRef](#)] [[PubMed](#)]
25. Batten, S.R.; Champness, N.R.; Chen, X.-M.; Garcia-Martinez, J.; Kitagawa, S.; Öhrström, L.; O’Keeffe, M.; Suh, M.P.; Reedijk, J. Terminology of metal–organic frameworks and coordination polymers (IUPAC Recommendations 2013). *Pure Appl. Chem.* **2013**, *85*, 1715–1724. [[CrossRef](#)]
26. Costa, B.A.; Nunes, W.D.G.; Bembo, L.H.; Siqueira, A.B.; Caires, F.; Leles, M.I.G.; Ionashiro, E.Y. Study of thermoanalytical behavior of heavier lanthanides terephthalates in air atmosphere. *J. Therm. Anal. Calorim.* **2018**, *134*, 1205–1210. [[CrossRef](#)]
27. Nunes, W.D.G.; Teixeira, J.A.; Do Nascimento, A.L.C.S.; Caires, F.J.; Ionashiro, E.Y.; Ionashiro, M. A comparative study on thermal behavior of solid-state light trivalent lanthanide isonicotinate in dynamic dry air and nitrogen atmospheres. *J. Therm. Anal. Calorim.* **2016**, *125*, 397–405. [[CrossRef](#)]
28. Daguebonne, C.; Kerbellec, N.; Guillou, O.; Bünzli, J.C.; Gumy, F.; Catala, L.; Mallah, T.; Audebrand, N.; Gérault, Y.; Bernot, K.; et al. Structural and Luminescent Properties of Micro- and Nanosized Particles of Lanthanide Terephthalate Coordination Polymers. *Inorg. Chem.* **2008**, *47*, 3700–3708. [[CrossRef](#)]

29. Kolesnikov, I.E.; Kolokolov, D.S.; Kurochkin, M.A.; Voznesenskiy, M.A.; Osmolowsky, M.G.; Lähderanta, E.; Osmolovskaya, O.M. Morphology and doping concentration effect on the luminescence properties of SnO₂:Eu³⁺ nanoparticles. *J. Alloys Compd.* **2020**, *822*, 153640. [[CrossRef](#)]
30. Haquin, V.; Etienne, M.; Daiguebonne, C.; Freslon, S.; Calvez, G.; Bernot, K.; Le Pollès, L.; Ashbrook, S.E.; Mitchell, M.R.; Bünzli, J.-C.; et al. Color and brightness tuning in heteronuclear lanthanide terephthalate coordination polymers. *Eur. J. Inorg. Chem.* **2013**, *2013*, 3464–3476. [[CrossRef](#)]
31. Kolesnikov, I.E.; Povolotskiy, A.V.; Mamonova, D.V.; Kolesnikov, E.Y.; Kurochkin, A.V.; Lähderanta, E.; Mikhailov, M.D. Asymmetry ratio as a parameter of Eu³⁺ local environment in phosphors. *J. Rare Earths* **2018**, *36*, 474–481. [[CrossRef](#)]

Disclaimer/Publisher’s Note: The statements, opinions and data contained in all publications are solely those of the individual author(s) and contributor(s) and not of MDPI and/or the editor(s). MDPI and/or the editor(s) disclaim responsibility for any injury to people or property resulting from any ideas, methods, instructions or products referred to in the content.